International Symposium
On Turbulence and Shear Flow
Phenomena (TSFP-9)
June 30 - July 3, 2015 *Melbourne, Australia*

SURFACE-MORPHOLOGY-INDUCED ENERGY REDISTRIBUTION IN TURBULENT BOUNDARY LAYERS

Marco Placidi*
Faculty of Engineering and the Environment
Aerodynamics and Flight Mechanics Group
University of Southampton
Highfield, Southampton, SO17 1BJ, UK
m.placidi@soton.ac.uk†

Bharathram Ganapathisubramani
Faculty of Engineering and the Environment
Aerodynamics and Flight Mechanics Group
University of Southampton
Highfield, Southampton, SO17 1BJ, UK
g.bharath@soton.ac.uk

ABSTRACT

Experiments were conducted in the fully-rough regime on surfaces consisting of regularly distributed Lego^{TM} bricks of uniform height ($h/\delta \approx 0.1$), arranged in different patterns. Measurements were made with both high-resolution particle image velocimetry and floating-element drag-balance on six surface morphologies with different frontal solidity, λ_F, and fixed plan solidity, λ_P. This paper complements results in Placidi & Ganapathisubramani (2013) and Placidi & Ganapathisubramani (2014) on the same rough surfaces.

Although the rough surfaces examined herein have shown a lack in outer-layer similarity (Placidi & Ganapathisubramani, 2013), current results based on proper orthogonal decomposition analysis indicates that some form of spatial universality of the flow is still present as significantly different rough morphologies exhibit virtually identical POD mode shapes and similar relative energy. The different percentages of the relative Turbulent Kinetic Energy (TKE) content in the first five POD modes strongly suggest that one of the effects of the surface morphology is to redistribute the energy across the turbulent scales. In particular, the effect of an increasing frontal solidity is to redistribute a larger proportion of the TKE to the larger-scales.

1 INTRODUCTION

Previous results on the same surface morphologies as those discussed herein have shown a lack of outer-layer similarity for higher-order statistics (Placidi & Ganapathisubramani, 2013). More specifically, while differences across cases in the mean velocity profiles were generally confined to the roughness sublayer (up to $5h$), the higher-order quantities, (i.e. the Reynolds stresses) have shown a lack of collapse across the entire wall-normal range. In contrast to Townsend's similarity hypothesis, these higher-order statistics showed dependency on the wall morphology. It is outside the scope of this paper to comment on the reasons for this lack of similarity. Nevertheless, further analysis on the same morphologies also revealed that the spatial structure of the turbulence is largely unaffected by a change in the wall surface (Placidi & Ganapathisubramani, 2014). The inclination angles of 2-point streamwise velocity correlations were found to be consistent not only across the cases studied herein but also when compared to the smooth-wall flows in the literature. This consistency was found to extend to velocity correlations shapes and extent. Therefore, it is clear that the turbulence above rough-wall boundary layers presents some universal characteristics, as largely discussed in the literature (Castro, 2007; Amir & Castro, 2011, among others).

To further explore this universality, the current paper focuses on the POD modes structures and energy contents at different turbulent scales. In particular, we investigate whether and to what extent the organisation of the turbulence is universal across the rough-walls studied herein, and what the effect of a change in surface morphology is on the energy distribution across the scales of the turbulence.

2 EXPERIMENTAL FACILITY AND DETAILS

The present experiments were carried out in a suction wind tunnel at the University of Southampton. The same facility has been used for previous rough-wall studies such as: Castro 2007; Reynolds & Castro 2008; Amir & Castro 2011; Claus *et al.* 2012. The tunnel has a working section of 4.5 m in length, with a $0.9\ m \times 0.6\ m$ cross section. The free-stream turbulence intensity is homogenous along the test section and less than 0.3%. In this study, the streamwise, wall-normal and spanwise directions are given along the $x-y-z$ directions and $u-v-w$ are the corresponding velocities. Fluctuating velocities are denoted with a $'$,

*Currently at City University London
†marco.placidi.1@city.ac.uk

while the letters are capitalised to represent the mean. Experiments were conducted at 11.5 m/s free-stream velocity in nominally zero-pressure-gradient as the acceleration parameter ($K = (\nu/U_e)[dU_e/dx]$) was less than 5×10^{-8}.

For rough surfaces, this study used a LEGO^{TM} baseboard onto which rectangular LEGO^{TM} bricks (or blocks), uniformly distributed in staggered array, were securely fixed. These bricks presented a uniform height ($h = 11.4$ mm). Six different patterns were adopted in order to systematically examine the individual effects of frontal solidity, λ_F (frontal area of the roughness elements per unit wall-parallel area), on the structure of the turbulence. More specifically, the plan solidity, λ_P (plan area of roughness elements per unit wall-parallel area), was kept constant whilst varying the λ_F. This condition was achieved by progressive repositioning of the roughness elements in the sheltered regions of the upstream obstacles. Figure 1 shows the basic repetitive units adopted to generate the different patterns in analysis. The reader is referred to Placidi (2015) for further details on the design rationale. A fetch length of about twenty times the boundary-layer thickness, δ, was covered with brick elements. Such a long fetch is necessary to guarantee that the boundary layers in examinations have reached the equilibrium and the fully-rough conditions, as from Castro (2007).

Measurements were taken at approximately 4 m downstream in the elements' field. Flow measurements were acquired using both planar and stereoscopic Particle Image Velocimetry (PIV). In both cases, the flow was seeded with vaporised glycol-water solution particles (1 μm in diameter) illuminated with a laser sheet produced by a pulsed New Wave Nd:YAG laser System operating at 200 mJ. Streamwise-wall-normal (x,y) planes were acquired at the spanwise centreline of the test section for the 2D case, whilst spanwise-wall-normal (z,y) planes were the object of the 3D measurements at the same location. The latter vector fields are used to check the spawise homogeneity of the flow given the high-relative roughness height ($h/\delta \approx 0.1$), however are not presented herein. 16 M *pixel* high resolution LaVision cameras equipped with Nikon 105 mm f/8 lenses were used. For each run, sets of 2000 pairs of digital images were captured and processed with *DaVis 8.0* software. The resulting spatial resolution is approximately 0.7 $mm \times 0.7$ mm (l^+ ranging in between 30 and 40) and successive vectors are spaced at half that distance (due to 50% overlap). The field of view (FOV) was cropped to approximately $1.5\delta \times 1\delta$ (streamwise-wall-normal) for the current analysis.

For the sake of completeness, a floating-element drag-balance inspired by Krogstad & Efros (2010) was designed and manufactured for the direct measurement of the skin-friction coefficient generated by the different wall conditions. The results of this high-accuracy balance compared well (within 10%) with skin friction predictions based on the total stress method as from both Reynolds & Castro (2008) and Manes *et al.* (2011). Once the skin friction velocity was calculated, a least-square-fit procedure was adopted to evaluate firstly the zero-plane displacement, d and then the roughness length, y_0. Further details on this procedure and a summary of these results can be found in Placidi & Ganapathisubramani (2013) and Placidi (2015), although these are not discussed in this paper, as they do not directly affect the conclusions drawn herein.

3 RESULTS AND DISCUSSION

The current study focuses on the universality of the turbulent structure and on the contributions of the different turbulent spatial scales towards the total TKE of the flow. To do so, a snapshot based POD has been carried out. Section 3.1 describes the technique applied, section 3.1.1 examines the global spatial structure of the flow over different types of roughness via analysis of POD modes shapes. The energy content of these modes is tackled in § 3.1.2 together with the effect of a varied frontal solidity on TKE. Finally some conclusions are drawn in § 3.1.3.

3.1 PROPER ORTHOGONAL DECOMPOSITION

Given the nature of our data set, it was convenient to apply a snapshot based POD (Berkooz *et al.*, 1993). This technique provides the most efficient way of identifying the motions which, on average, contain a majority of the TKE in the flow (Palmer *et al.*, 2011).

The energy contribution of the singular value across the modes, hence its shape, depends on the local spatial resolution of the data set, as discussed in Pearson *et al.* (2013). This is because the energy content of each ϕ_i mode depends on the smallest resolved scale in the flow. The spatial resolution of the current 2D data set ranges in between 30 to 40 wall-units, resulting in a variation of the Kármán number in the range of $Re_\tau \approx 5000 - 7300$. Therefore, a low-pass Gaussian filter, designed to match the local resolution at $l^+_{2D} = 45$ is applied to all cases. Moreover, the Field Of View (FOV) across the different morphologies is also matched to allow meaningful comparisons. The smallest scales in the flow can be assumed to be of the order of the Kolmogorov length scale. Following Kolmogorov (1941), this scale was estimated to be $\eta = 0.1$ mm. This corresponds to $l^+_{2D} \approx 4-6$ based upon the different skin-friction velocities at a wall-normal location $y/\delta \approx 0.4$. Therefore, the current data set is resolved, in the worst case, down to approximately 7 times the Kolmogorov's length scale (based on $l^+_{2D} = 45$). It must also be noted that this filtered spatial resolution is comparable (if not better) than previous cross-wire and PIV based measurements presented in the literature.

3.1.1 POD modes shapes Figure 2 shows contour plots of the shape of the first five POD modes for increasing λ_F (sparse, medium-packed and dense regimes from left to right). Regions of high and low streamwise momentum are highlighted in black and white respectively, although the colorbar is arbitrary.

It can be clearly seen in figure 2 that the mode characteristics are found to be consistent and indistinguishable in both shape and order across all surface morphologies, regardless of the regime. This level of consistency is remarkable considering the different wall conditions (see figure 1) and is a clear testimony of a form of spatial universality of the turbulence structure over rough-walls. It is important to note that, although the flows were shown (Placidi, 2015) to be dependent on the wall surface in the roughness sublayer (RSL), none of this inhomogeneity is found in the POD modes shapes calculated over the entire boundary layer thickness. This is due to the energy in the outer-region which seems to dominates the overall kinetic energy.

The shape of the most energetic mode, mode 1, is characterised by an elongated large scale high-momentum region. Mode 2 shows an inclined shear layer that separates a

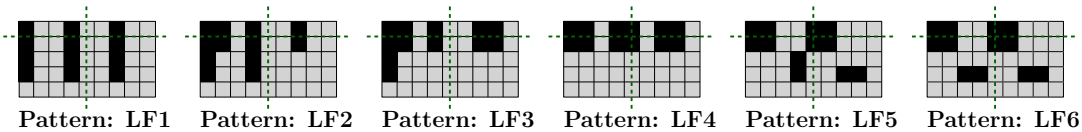

Figure 1. Roughness elements' patterns with varying λ_F at $\lambda_P = const = 0.27$. Flow is top to bottom. Dashed lines indicate the location of the laser sheets during the data acquisition for both 2D and 3D setups.

Table 1. Relevant experimental parameters.

Data set	λ_F	λ_P	$\delta(mm)$	$\delta^*(mm)$	h/δ	$U_\tau(m/s)$	Re_τ	d/h	y_0/h
LF1	0.09	0.27	111	19	0.10	0.65	5000	0.98	0.02
LF2	0.12	0.27	122	27	0.09	0.73	6100	0.59	0.05
LF3	0.15	0.27	121	26	0.09	0.71	5900	0.80	0.04
LF4	0.18	0.27	122	28	0.09	0.80	6700	0.75	0.10
LF5	0.21	0.27	129	32	0.09	0.82	7300	0.61	0.12
LF6	0.24	0.27	127	31	0.09	0.81	7100	0.73	0.11

high-momentum region below it from a low-momentum region appearing above it. Similar shape is assumed by mode 3, but the inclination of the shear layer appears reversed. Mode 4 is dominated instead by three distinctive regions. Two localised high-momentum regions are separated by an elongated forward leaning streamwise low-momentum region. Finally, mode 5 is characterised by four alternating regions of low and high momentum. These regions are smaller than the ones characterising the previous modes.

A trend of increasingly smaller structures for higher modes is generally found throughout all cases. Therefore, the most energetic modes tend to be associated with large-scale structure, whilst later modes are representative of increasingly smaller-scales. This behaviour has been well-documented (Holmes *et al.*, 1996). This trend can be visualised by plotting the correlation coefficient between the $1st$-mode and the ϕ_{i-th}-mode for the same (λ_F or λ_P) case. Figure 3 shows the result of this procedure. As expected, by definition, the correlation coefficient is unity for mode 1 (auto-correlation), while decreases for increasing order of the mode. This is true across all cases.

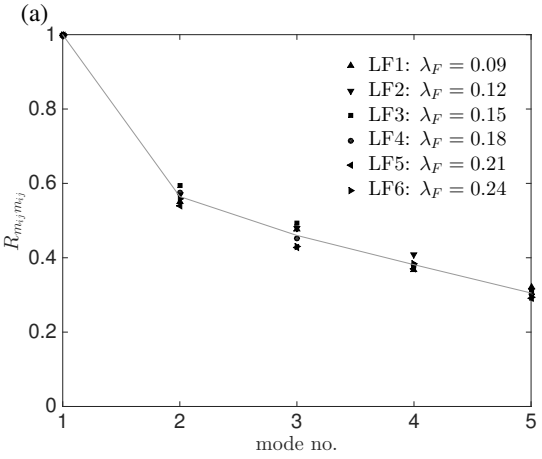

Figure 3. Correlation coefficient, $R_{m_i m_i}$ as a function of λ_F ($\lambda_P = const = 0.27$). POD modes are calculated on the combined (u', v') field. Grey lines indicate the trend.

3.1.2 POD modes energy content More quantitative information can be gathered by investigating the fractional and cumulative TKE FTKE and CTKE, repsectively) mode contributions. Table 2 shows the FTKE contribution to the total TKE for all the λ_F cases. It can be seen that cases with lower λ_F tend to be characterised by lower energy content in the first POD mode. Therefore low-order modes contain, on average, more energy for the dense cases compared to the sparse cases. For example, mode 1 for the LF1 case contains only $\approx 15\%$ of the total energy, while for the LF3 and LF6 cases, its content reaches $\approx 16\%$ and $\approx 18\%$, respectively. Moreover, the CTKE of the first five modes contributes to $\approx 38\%$ of the total TKE for the densest case, LF6, while it only represent contributions of $\approx 34\%$ for the sparsest case, LF1. This further confirms that an increased frontal solidity results in a redistribution of energy towards larger scales (or lower-order modes).

The same trend can also be inferred from the number of modes necessary to contribute to 50% of the total turbulent kinetic energy, which is progressively lower for increasing λ_F. Although not considered here, the reader's attention is also drawn to the fact that more than 800 modes are needed to capture 95% of the total TKE of the flow. This reflects the complexity and the wide range of statistically important spatial scales present in the flow at these Reynolds numbers.

The results presented so far clearly suggest that the effect of an increased frontal solidity would be to redistribute the energy toward the highest energy POD modes. This is an indication of an increase in energetic coherent turbulent structures in the denser regimes, which could be responsible for the lack of outer layer similarity in Placidi & Ganapathisubramani (2013).

3.1.3 POD of isolated velocity fluctuations Having investigated the behaviour of the POD modes calculated from the (u', v') combined velocity field,

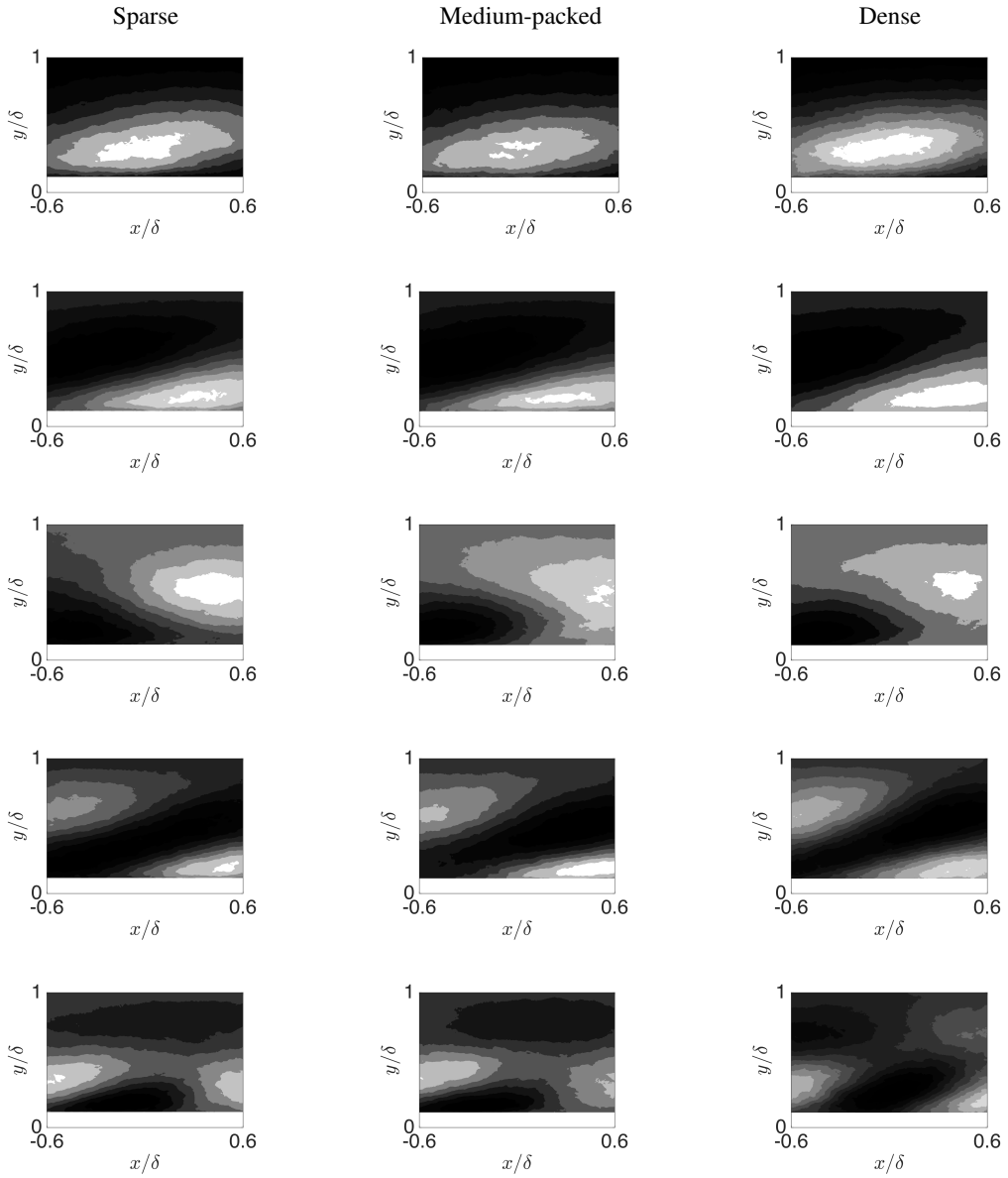

Figure 2. First five low-order POD modes for increasing λ_F ($\lambda_P = const = 0.27$). Cases: LF2 (left), LF3 (centre-left), LF5 (right). POD modes order increases from top to bottom. Flow is left to right. POD modes are calculated on the combined (u', v') field.

further information for each velocity component can be obtained calculating the modes solely from the (u') or (v') fields. Similar boundaries as for the combined case are chosen for the vertical and horizontal extend of the FOV. When POD modes are calculated over the (u') field, for both λ_F and λ_P, their shapes are remarkably similar to those for the combined field in figure 2, and hence not shown. This is to be expected as the combined field matrix is constructed with the streamwise velocity first - it is therefore reasonable that this component are more represented in the first low-order POD shapes. It is perhaps more interesting to investigate the behaviour of the (v') field. This should be different from the previous case and can reveal new insight on the effect of surface morphology on the wall-normal structures. Figure 4 shows contour plots of the shape of the first five POD modes for an increase in both λ_F (as for the previous case), calculated solely upon this simplified wall-normal velocity field. It is striking that, although mode 1 results are similar to the previous case (in figure 2), from mode 2 onward the POD modes have very different shapes compared to the previous results. It is perhaps not surprising that the mode structures for the wall-normal field are much smaller and compact, in agreement with snapshots of instantaneous wall-normal velocity fields, which are very localised, compact and small-scale dominated (as well documented in the literature). It is also worth noting that the correspondence of mode number/shape across cases seems to break down after mode 4, where the similarity across cases is lost. This is probably due to the higher localised effect the canopy layer has on the wall-normal velocity fluctuations (when compared to the streamwise).

Finally, table 3 shows the POD mode energy content based on the isolated (v') field. Although the actual values of the FTKE and CTKE are different from the previous

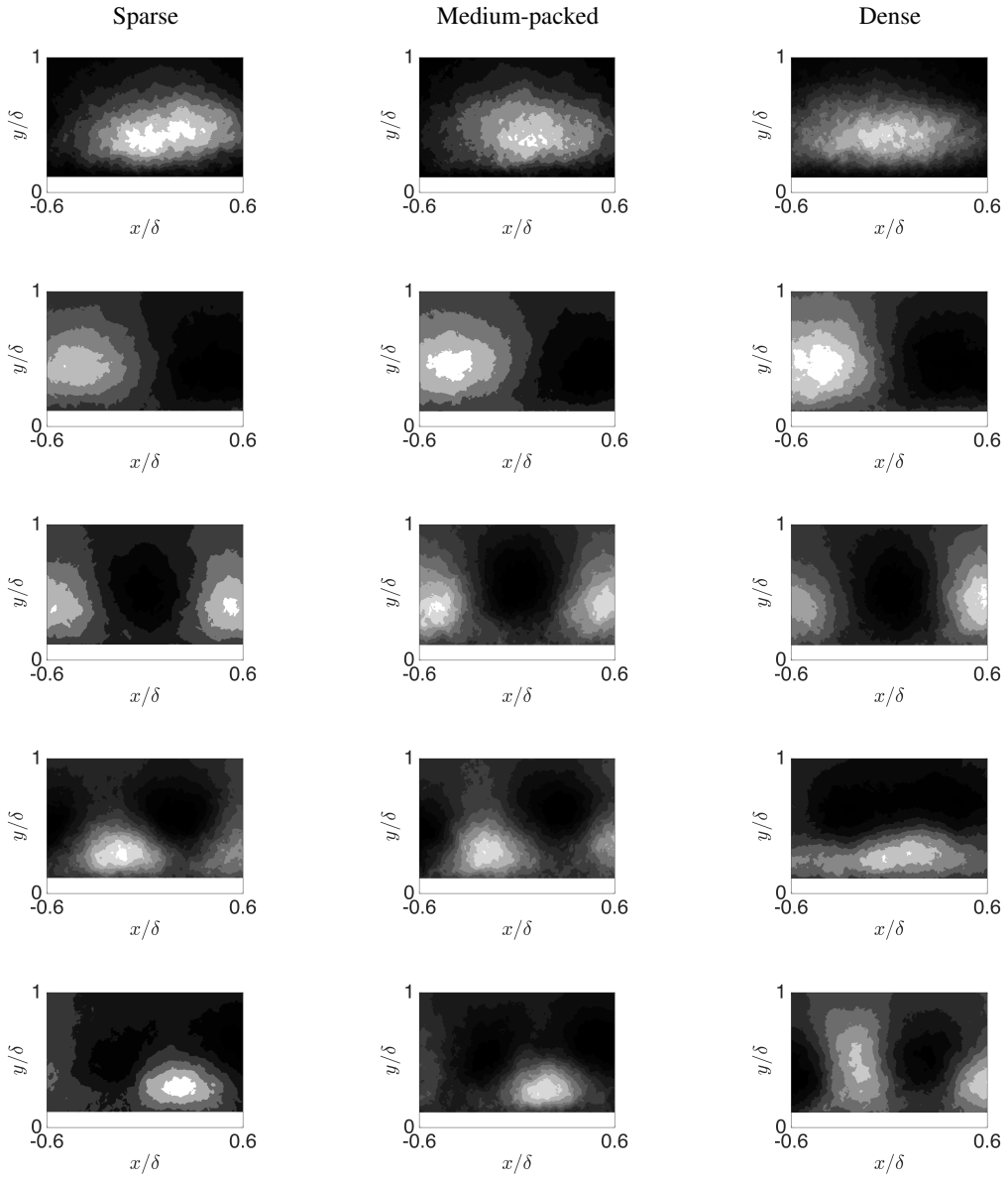

Figure 4. First five low-order POD modes for increasing λ_F ($\lambda_P = const = 0.27$). Cases: LF2 (left), LF3 (centre-left), LF5 (right). POD modes order increases from top to bottom. Flow is left to right. POD modes are calculated on the (v') field only.

Data set	E_1	E_2	E_3	E_4	E_5	$\sum_{i=1}^{5} E_i$	$0.5\sum_{i=1}^{n} E_i$
LF1	15	7	5	4	3	34	17
LF2	16	8	5	5	3	37	14
LF3	16	8	6	4	3	36	14
LF4	16	8	5	4	3	36	14
LF5	18	8	5	4	3	38	12
LF6	18	8	5	4	3	38	12

Table 2. Fractional TKE, E_i and cumulative TKE $\sum_{i=1}^{n} E_i$ content versus mode number. $0.5\sum_{i=1}^{n} E_i$ refers instead to the number of modes necessary to resolve the 50% of the turbulent kinetic energy contained in the flow. POD modes are calculated on the combined (u', v') field.

case in table 2, the trends are very similar. Therefore the energy redistribution process previously described is found to be robust even when isolated velocity components are considered. Again, the relative energy content in the POD modes strongly suggest that the effect of increasing λ_F is to redistribute a larger proportion of the energy to the highest energy POD modes (i.e. the larger-scales).

CONCLUSIONS

As discussed in § 1, previous results on the same surface morphologies have shown that a lack of outer layer similarity characterises the high-order turbulent statistics (Placidi & Ganapathisubramani, 2013). However, we also previously shown that the spatial organisation of the turbulence (i.e. inclination of velocity correlations and associated length scales) is consistent across all the different wall conditions (Placidi & Ganapathisubramani, 2014). The

Data set	E_1	E_2	E_3	E_4	E_5	$\sum_{i=1}^{5} E_i$	$0.5\sum_{i=1}^{n} E_i$
LF1	5	4	3	2	2	17	48
LF2	6	5	4	3	3	20	38
LF3	6	5	4	3	2	19	42
LF4	6	5	4	3	2	19	43
LF5	7	5	4	3	3	22	31
LF6	7	5	4	3	3	21	33

Table 3. Fractional TKE, E_i and cumulative TKE $\sum_{i=1}^{n} E_i$ content versus mode number. $0.5\sum_{i=1}^{n} E_i$ refers instead to the number of modes necessary to resolve the 50% of the turbulent kinetic energy contained in the flow. POD modes are calculated on the (v') field only.

current findings complement previous results. In particular we strengthen our latest work' conclusions in favour of a universal organisation of the turbulence across rough-wall boundary layers. It was also demonstrated that the POD technique can effectively be used to infer similarity in the spatial organisation of the flow over different morphologies. Finally, it is also shown that an increase in λ_F is accompanied by a redistribution of energy toward the lower-order modes (i.e. large-scale), which results in enhanced energetic large-scale coherent structures.

ACKNOWLEDGEMENTS

We gratefully acknowledge the support from the European Research Council under the European Union's Seventh Framework Programme (FP7/2007-2013) / ERC Grant agreement No. 277472. We also thank Lloyd's Register Foundation (LRF) as well as the Faculty of Engineering and the Environment for supporting this research.

REFERENCES

Amir, M & Castro, I P 2011 Turbulence in rough-wall boundary layers: universality issues. *Experiments in Fluids* **51**, 313–326.

Berkooz, G, Holmes, P & Lumley, J L 1993 The proper orthogonal decomposition in the analysis of turbulent flows. *Annual Review of Fluid Mechanics* **25**, 539–575.

Castro, I P 2007 Rough-wall boundary layers: mean flow universality. *Journal of Fluid Mechanics* **585**, 469–485.

Claus, J, Krogstad, P A & Castro, I P 2012 Some Measurements of Surface Drag in Urban-Type Boundary Layers at Various Wind Angles. *Boundary-Layer Meteorology* **145** (3), 407–422.

Holmes, P, Lumley, J L & Berkooz, G 1996 *Turbulence, Coherent Structures, Dynamical Systems and Symmetry*. Cambridge University Press.

Kolmogorov, A N 1941 The local structure of turbulence in incompressible viscous fluids at very large Reynolds numbers. *Dokl. Akad. Nauk. SSSR. Reprinted in Proc R Soc London A 434, 9-13 (1991)* **30**, 299–303.

Krogstad, P A & Efros, V 2010 Rough wall skin friction measurements using a high resolution surface balance. *International Journal of Heat and Fluid Flow* **31** (3), 429–433.

Manes, C, Poggi, D & Ridolfi, L 2011 Turbulent boundary layers over permeable walls: scaling and near-wall structure. *Journal of Fluid Mechanics* **687**, 141–170.

Palmer, J A, Mejia-Alvarez, R, Best, J L & Christensen, K T 2011 Particle-image velocimetry measurements of flow over interacting barchan dunes. *Experiments in Fluids* **52** (3), 809–829.

Pearson, D S, Goulart, P J & Ganapathisubramani, B 2013 Turbulent separation upstream of a forward-facing step. *Journal of Fluid Mechanics* **724**, 284–304.

Placidi, M 2015 On the effect of surface morphology on wall turbulence. PhD thesis, University of Southampton. Engineering and the Environment.

Placidi, M & Ganapathisubramani, B 2013 Investigation of wall-bounded turbulence over regularly distributed roughness. In *8th International Symposium on Turbulence and Shear flow phenomena, Poitiers, France August 28–30*.

Placidi, M & Ganapathisubramani, B 2014 On the effects of surface morphology on the structure of wall-turbulence. In *interdisciplinary Turbulence initiative, Bertinoro, Italy September 21-24.*, pp. 1–4.

Reynolds, R T & Castro, I P 2008 Measurements in an urban-type boundary layer. *Experiments in Fluids* **45**, 141–156.